A methodology for identifying information rich frequency bands for diagnostics of mechanical components-of-interest under time-varying operating conditions

Stephan Schmidt[a,*], Alexandre Mauricio[b,c], P. Stephan Heyns[a], Konstantinos C. Gryllias[b,c]

[a] *Centre for Asset Integrity Management, Department of Mechanical and Aeronautical Engineering, University of Pretoria, Pretoria, South Africa*
[b] *Department of Mechanical Engineering, KU Leuven, Celestijnenlaan 300, 3001 Heverlee, Belgium*
[c] *Dynamics of Mechanical and Mechatronic Systems, Flanders Make, Belgium*

Abstract

Performing condition monitoring on rotating machines such as wind turbines, which operate inherently under time-varying operating conditions, remains a challenge. The signal components generated by incipient damage are masked by other signal components that are not of interest and high noise levels. In this work, a new method, referred to as the IFBI$_\alpha$gram, is proposed that is capable of identifying frequency bands that are rich with diagnostic information related to specific cyclic components. This allows the optimal frequency band to be determined for diagnosing the component-of-interest. It is shown on numerical and experimental gearbox data that this method is not only capable of detecting incipient damage, but is also robust to time-varying operating conditions. Therefore, it can be used to independently determine the condition of different mechanical components and it is robust to spurious transients.

Keywords:
Gearbox diagnostics, Time-varying operating conditions, Frequency Band Identification, IFBI$_\alpha$gram, Cyclostationarity

1. Introduction

Detecting incipient damage is extremely important for critical machines such as wind turbines [1–3] and helicopters [4, 5] and remains a very challenging task. The interaction

*Corresponding author.
Email address: stephan.schmidt@up.ac.za (Stephan Schmidt)

of various mechanical components (e.g. gear meshing) and the fact that these machines often operate in noisy environments under time-varying operating conditions, impede the ability of conventional fault detection techniques to perform effectively, i.e. detecting damage early [6–8].

In a damaged machine such as a gearbox, impulses are typically generated when the damaged part of the component such as the inner race of a bearing moves in and through the loading zone. Due to the cyclical nature of the rotating components, these impulses generate cyclostationary signals [9]. These impulses also excite the structure of the machine and ultimately manifest in specific spectral frequency bands [10], which are dependent on the properties of the system and independent of the operating conditions. The excitation of the spectral frequency bands at specific cyclic orders means that the signal can be approximated as angle-time cyclostationary under time-varying speed conditions [11–14].

Signal enhancement techniques (e.g. [15, 16]) and analysing bandlimited signals [17], which only contain information pertaining to the component of interest, can be used to aid incipient fault detection. Synchronous averaging [6, 18], envelope analysis [19], time-frequency analysis and related techniques [20–23] are very popular methods to highlight the damage components in the data of rotating machines. Techniques that aim to identify frequency bands with diagnostic information, which can ultimately be used to obtain bandlimited signals, are referred to as Frequency Band Identification (FBI) techniques in this paper.

The most notable FBI tool is the spectral kurtosis, where essentially the kurtosis of different bandlimited signals is used to identify frequency bands with impulsive information [24, 25]. The extensive theoretical development of the spectral kurtosis in Ref. [24, 25] has allowed its use as an FBI technique and also as a filter to amplify the impulsive information [26]. The Short-Time Fourier Transform (STFT) can be used to estimate the spectral kurtosis, however, the spectral kurtosis is sensitive to the window length that is used in the STFT estimation. Hence, Antoni and Randall [24] proposed the kurtogram, where the spectral kurtosis is estimated from the STFT, calculated for different window lengths, and ultimately maximised to obtain the centre frequency and the bandwidth that is best for detection. The repeated application of the STFT can be time-consuming and therefore

Antoni [27] proposed the fast kurtogram, which uses a wavelet packet decomposition instead of the STFT as an estimator for the spectral kurtosis to ultimately obtain the kurtogram. The additional benefit of the fast kurtogram is that it uses a 1/3-binary tree to obtain a feature plane with a much better resolution. The spectral kurtosis and the kurtogram have been very successful for bearing [24] and gear fault diagnosis [26, 28].

The kurtogram, however, also has its shortcomings. It cannot distinguish between a single transient and repetitive transients and its values are dependent on the cyclic frequency, e.g. as the rotating speed of the machine increases, the kurtosis decreases [24, 29]. Hence, many improvements have been proposed [29, 30]. Much research effort has been devoted to using statistics from the frequency domain instead of the time domain for detecting repetitive transients, such as the protrugram [30], the enhanced kurtogram [31], the sparsogram [32], the optimised spectral kurtosis [33] and the infogram [29, 34]. Xu et al. [35] proposed the envelope-to-harmonic ratio for extracting periodic transients. Moshrefzadeh and Fasana [36] proposed the autogram, which calculates the kurtosis of the unbiased autocorrelation function as a feature. Borghesani et al. [37] related envelope and kurtosis-based indices and proposed a ratio of cyclic content metric that includes information related to the kinematics of the component-of-interest for automatic demodulation band identification. Smith et al. [38] proposed the ICS2gram which uses an indicator of cyclostationarity to identify frequency band with strong cyclostationary information related to the component-of-interest. Mauricio et al. [39, 40] proposed the IESFOgram, which uses the spectral coherence, the improved envelope spectrum and a feature to determine the frequency band that results in an optimal improved envelope spectrum for detecting specific damage components. Schmidt et al. [41] proposed a methodology to combine historical data from a healthy machine with FBI techniques. Smith et al. [42] recently did a comparative study between different conventional FBI methods and made the distinction between blind (i.e. without using any prior knowledge about the kinematics of the machine) and targeted (e.g. techniques such as the ICS2gram [38] and the IESFOgram [39, 40]) methods. The results indicate that the targeted methods are much better for detecting damage [42].

However, extracting a metric such as the kurtosis from the time-domain or the cyclic spectrum of a bandlimited signal only allows the frequency band which maximises the

metric to be identified, e.g. the impulsivity, and does not distinguish between the different events that contribute to the impulsivity. Hence, the identified frequency band may not be of interest (e.g. impulsive noise) or may only be optimal to detect the most dominant component and not necessarily the weak component-of-interest.

An FBI methodology is therefore proposed in this work to identify the optimal frequency band to detect a set of predetermined cyclic components $\{\alpha_f\}$ under time-varying operating conditions. This methodology is referred to as the IFBI$_\alpha$gram (Information rich Frequency Band Identification), with the subscript α emphasising that it is determined for specific cyclic components. The set of cyclic components, denoted $\{\alpha_f\}$, can for example be the Ball-Pass Order Outer (BPOO) race component and its harmonics, i.e. $\{\alpha_f\} = \{1 \cdot \text{BPOO}, 2 \cdot \text{BPOO}, 3 \cdot \text{BPOO}\}$.

In summary, the benefits of the proposed IFBI$_\alpha$gram are as follows:

- Information rich frequency bands that are optimal too detect specific cyclic components in the set $\{\alpha_f\}$ can be automatically identified.
- The IFBI$_\alpha$gram can be used to detect various damage modes, which may simultaneously be present in the rotating machine.
- It is possible to combine the IFBI$_\alpha$gram with advanced signal analysis techniques for detecting damage under time-varying operating conditions.

In this work, the IFBI$_\alpha$gram is compared to the fast kurtogram, because the kurtogram is a well established technique that has been used for gear and bearing diagnosis and prognosis under constant and time-varying operating conditions [3, 24–28]. However, in Section 4.5, a brief comparison is also made with the ICS2gram to further emphasise the benefits of using the proposed methodology. In summary, the novel contributions of this work are as follows:

- A novel frequency band identification technique, referred to as the IFBI$_\alpha$gram, is proposed for gearbox fault diagnosis under time-varying operating conditions. The IFBI$_\alpha$gram is calculated by combining the order-frequency spectral coherence with a signal-to-noise ratio feature.

- The repeated use of the order-frequency spectral coherence instead of the STFT allows targeted features to be extracted that are unaffected by the bias in the estimators due to the time-frequency limitations (e.g. the cyclic spectrum derived from the STFT is a biased estimator).

- The methods are analysed on gearbox data that were acquired under time-varying operating conditions in the presence of impulsive noise.

- In the calculation of the signal-to-noise ratio feature, it is shown that by normalising the feature by the median instead of the average and the root-mean-square, it is possible to have a more robust estimation of the noise level when the signal contains much cyclostationary information.

The layout of the paper is as follows: The IFBI$_\alpha$gram is presented in Section 2, whereafter it is evaluated on numerical gearbox data in Section 3 and experimental gearbox data in Section 4. In Appendix A, supporting information is provided to motivate using the median in the feature proposed in Section 2.2, while Appendix B contains additional information related to the numerical gearbox model used in Section 3.

2. The IFBI$_\alpha$gram

The process diagram of the calculation of the IFBI$_\alpha$gram is given in Figure 1. A

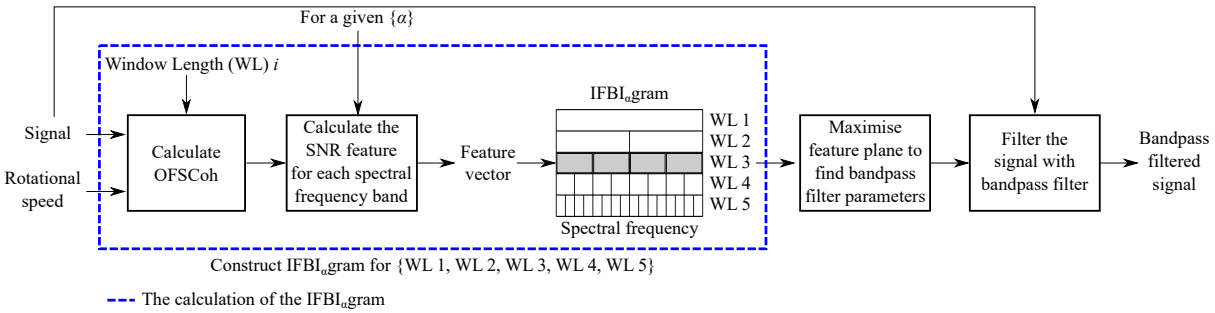

Figure 1: An overview of the methodology that utilises the proposed IFBI$_\alpha$gram to obtain a bandlimited signal which can be used for fault diagnosis. This procedure needs to be performed separately for each measurement in the dataset.

vibration signal and the corresponding rotational speed $\omega(t)$ (or the instantaneous phase $\theta(t)$) of a shaft in the system are used as inputs, whereafter an Order-Frequency Spectral

Coherence (OFSCoh) is calculated for each Window Length (WL) that is considered. The window length is directly linked to the spectral frequency resolution of the OFSCoh and therefore they can be used interchangeably. After the OFSCoh is calculated for a specific WL, a feature, which is dependent on $\{\alpha_f\}$, is extracted from each spectral frequency band of the OFSCoh and is used to construct the feature plane. Thereafter, the feature plane is maximised to obtain the bandpass filter parameters that are used to extract the bandlimited signal. This bandlimited signal is rich with diagnostic information pertaining to $\{\alpha_f\}$ and can be analysed to infer the condition of the machine.

A more detailed overview of each step is given in the subsequent sections.

2.1. Calculation of the OFSCoh

The Order-Frequency Spectral Coherence (OFSCoh) of the vibration signal $x(t)$ [13]

$$\gamma_{xx}(\alpha, f) = \frac{S_{2x}(\alpha, f)}{\left(S_{2x_\alpha}(0, f) \cdot S_{2x}(0, f)\right)^{1/2}}, \tag{1}$$

is a function of the Order-Frequency Spectral Correlation (OFSC) of the signal [13]

$$S_{2x}(\alpha, f) = \lim_{T\to\infty} \frac{1}{\theta(T) - \theta(0)} \mathbb{E}\left\{\mathcal{F}_T\left(x(t)\right)^* \cdot \mathcal{F}_T\left(x(t)e^{-j\alpha\theta(t)}\omega(t)\right)\right\}, \tag{2}$$

where T is the time-period of the signal, $\mathcal{F}_T$ is the Fourier transform over a period T and $\omega(t) = \frac{d}{dt}\theta(t)$. This allows the bandlimited impulses to be represented in terms of cyclic orders α and spectral frequencies f and can therefore be used to identify information rich frequency bands related to specific mechanical components. The OFSCoh has been successfully used for bearing and gear fault detection under time-varying operating conditions [13, 40, 43]. The benefit of using the OFSCoh, a normalised form of the OFSC, is that it is able to amplify weak components in the signal [13] and is therefore ideal for fault detection problems. Hence, it is used as a first step in this method. Utilising the OFSCoh in this methodology ensures that it is possible to detect weak components in the signal and it makes the method well-suited for applications under time-varying operating conditions.

However, estimators need to be used to calculate Equation (2) for measured signals. The Welch estimator has very good bias and variance properties when compared to other conventional estimators [44] and is therefore used in this work. It is implemented using

the procedure proposed in Ref. [13]. Recently, faster estimators of the spectral correlation have been proposed in Refs. [45, 46] which would make the calculation of the IFBI$_\alpha$gram more computationally efficient.

2.2. Feature extraction and feature plane construction

The objective is using the OFSCoh to determine a frequency band $[f-\Delta f/2, f+\Delta f/2]$, which maximises the diagnostic information related to a specific cyclic component. This is performed by extracting a feature that is a function of $\{\alpha_f\}$ from each spectral frequency band in the OFSCoh and using the extracted features to construct a feature plane. The estimated OFSCoh, with a frequency resolution of Δf, is denoted $\hat{\gamma}_{xx}(\alpha, f; \Delta f)$. The resulting feature plane for $\{\alpha_f\}$

$$\Psi_{xx}(f, \Delta f; \{\alpha_f\}) = \sum_{\alpha \in \{\alpha_f\}} \mathrm{SNR}\left\{|\hat{\gamma}_{xx}(\alpha, f; \Delta f)|^2\right\}, \tag{3}$$

is constructed based on a signal-to-noise ratio measure

$$\mathrm{SNR}\{X(\alpha)\} = \frac{\mathcal{A}\{X(\alpha)\}}{\mathcal{G}\{X(\alpha)\}}, \tag{4}$$

where $\mathrm{SNR}\{X(\alpha)\}$ is a measure of the signal-to-noise ratio of the spectrum $X(\alpha)$ at a cyclic order of α. The dependence of the function $X(\alpha)$ on other parameters such as the spectral frequency is omitted in Equation (4). The operator $\mathcal{A}\{\cdot\}$ in Equation (4) calculates the magnitude of the cyclic component α under consideration and $\mathcal{G}\{\cdot\}$ estimates the noise level at the cyclic order of α. The feature in Equation (4) can therefore be used to identify the frequency band in which the cyclic component α is most prominent. The metric in Equation (4) is inspired from the quality metric that was used in Ref. [41] to estimate the diagnostic information in the Squared Envelope Spectra (SES) of a signal.

Since the analytical cyclic order may be slightly different than the actual cyclic order and since the noise level is not available, estimators need to be used for $\mathcal{A}\{\cdot\}$ and $\mathcal{G}\{\cdot\}$. The function $\mathcal{A}\{\cdot\}$ is estimated by assuming that for $\alpha \in [\alpha_f \cdot (1-d), \alpha_f \cdot (1+d)]$ only the signal component-of-interest is present, where $d = 0.01$ is used for all cases. This signal component would be larger than the surrounding noise and therefore the maximum value of the data in the band $\alpha \in [\alpha_f \cdot (1-d), \alpha_f \cdot (1+d)]$ is assumed to be the component-of-interest. If $d \neq 0$, it means that deviations from the theoretical or analytical cyclic orders of the cyclic component-of-interest are allowed.

The noise level function $\mathcal{G}\{\cdot\}$ is estimated by calculating the median in the band $\alpha \in [\alpha_f - 1, \alpha_f + 1]$. The median is calculated in this band to ensure that there are sufficient data to properly estimate this noise level without, for example, being affected by roll-off effects or other signal components. The range of this band can be increased, but this will increase the computational time of the IFBI$_\alpha$gram and may lead to inaccurate estimations if the noise level is a strong function of cyclic orders, e.g. if a roll-off phenomenon is present. The median, as a method to estimate the noise level, is properly motivated in Appendix A. The median was also used in Refs. [41, 47] to estimate the noise level in a cyclic spectrum (e.g. SES).

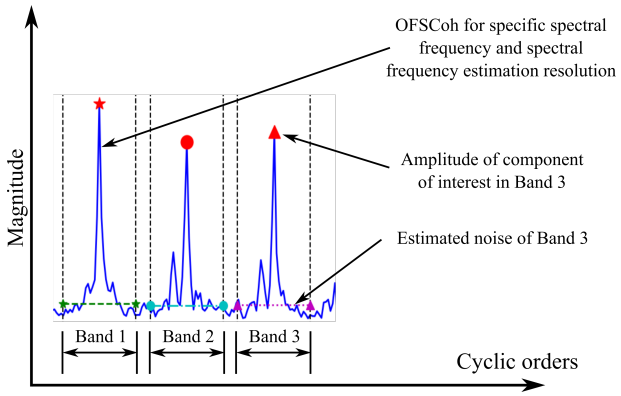

Figure 2: The different components, used in the calculation of the feature in Equations (3) and (4), are shown for the case where the cardinality of $\{\alpha_f\}$ is three. The amplitudes are estimated with $\mathcal{A}$ and the noise level is estimated with $\mathcal{G}$, with the band that is used in the estimation of the noise level of each harmonic being shown as well.

The different components of Equation (3) are visualised in Figure 2 for the OFSCoh in a specific spectral frequency band. Even though the OFSCoh is used in this example, the feature in Equation (4) can be combined with the Squared Envelope Spectrum (SES) of a processed signal as a simple method to perform fault trending, i.e. Equation (3) is calculated for the SES instead of the OFSCoh. This is similar to the quality metric used in Ref. [41].

2.3. Feature plane maximisation

The feature plane can be constructed by calculating the feature in Equation (3) for different spectral frequency bands f and different frequency resolutions Δf, obtained by using different window lengths in the estimation of the OFSCoh. The objective is to find

the frequency band $[f - \Delta f/2, f + \Delta f/2]$, which is optimal to detect the cyclic orders in the set $\{\alpha_f\}$, with

$$\arg\max_{f,\Delta f} \Psi_{xx}(f, \Delta f; \{\alpha_f\}). \tag{5}$$

Hence, the spectral frequency f and the spectral frequency resolution Δf (or equivalently the window length) that maximise the feature plane are identified and then used to design a bandpass filter. The filtered or bandlimited signal $x(t; f, \Delta f)$, obtained after applying the bandpass filter to the original signal, can subsequently be analysed to infer the condition of the machine.

2.4. Analysis of the bandpass filtered signal

There are many signal processing and analysis methods that can be used to interrogate raw and filtered signals for damage [10, 48]. The Synchronous Average of the Squared Envelope (SASE) for a given period Φ_0

$$s_x(\varphi; \Phi_0) = \frac{1}{N_0} \sum_{k=0}^{N_0-1} |x(\varphi + k \cdot \Phi_0)|^2, \tag{6}$$

can be used to detect the synchronous patterns in the instantaneous power of the order tracked signal, attributed to the impulses that are generated from the damaged component. The SASE is also very useful to visualise the condition of the gear and to evaluate the extent of the damage [17, 18, 49]. The period of the SASE in rotations, i.e. $\Phi_0/(2\pi)$, is the reciprocal of the fundamental cyclic order of the component-of-interest.

The SES [19]

$$\mathrm{SES}(\alpha; f, \Delta f) = \underset{\varphi \to \alpha}{\mathcal{F}} \left\{ \mathbb{E} \left\{ |x\left(t(\varphi); f, \Delta f\right)|^2 \right\} \right\}, \tag{7}$$

is one of the most powerful techniques for bearing diagnostics [10, 19] and can be used for gear diagnostics [41] as well. This can be used to determine the presence of specific damage components in the signal and to support the inferences made with the SASE.

The spectral coherence is a two-dimensional representation of a signal in terms of the spectral frequencies and the cyclic frequencies. However, it is simpler to use a spectrum when inferring the condition of the machine and therefore the Enhanced Envelope Spectrum (EES)

$$\mathrm{EES}(\alpha) = \frac{1}{f_s/2} \int_0^{f_s/2} |\gamma_{xx}(\alpha, f)|^2 df, \tag{8}$$

can be used. The integration over the whole frequency band $[0, f_s/2]$ could mask weak components in the spectrum and therefore the Improved Envelope Spectrum (IES) [14]

$$\mathrm{IES}(\alpha; f, \Delta f) = \frac{1}{\Delta f} \int_{f-\Delta f/2}^{f+\Delta f/2} |\gamma_{xx}(\alpha, f)|^2 df, \tag{9}$$

can be used to highlight the weak components better if the frequency range of integration, i.e. $[f - \Delta f/2, f + \Delta f/2]$, is carefully selected. However, the frequency band needs to be specified before the IES can be calculated. In this work, the estimated frequency band, obtained with a FBI method, is also used to select the IES in Section 4.3.

Even though the raw and filtered signals are used in this paper, signal enhancing techniques such as Cepstrum Pre-Whitening (CPW) [16] and the Generalised Synchronous Average (GSA) [15] can be used to remove the healthy deterministic components (e.g. gear mesh components) and retain the random components attributed to damage. This is illustrated in Section 4.3.2, where the EES and the IES are calculated from the OFSCoh of the CPW signal to diagnose the gears.

In the next section, the proposed IFBI$_\alpha$gram is investigated and compared to the fast kurtogram on numerical gearbox data.

3. Numerical investigation

In this section, the proposed IFBI$_\alpha$gram is compared to the fast kurtogram on numerical gearbox data generated with a phenomenological gearbox model. An overview of the phenomenological gearbox model and the considered data are given in Section 3.1, whereafter the IFBI$_\alpha$gram is investigated in Section 3.2 and the fast kurtogram is investigated in Section 3.3. The main purposes of this investigation are to illustrate the following:

- The proposed method can be used to detect weak components that are masked by more dominant components.
- The proposed method can distinguish between repetitive and non-repetitive transients.

3.1. Phenomenological gearbox model

The phenomenological gearbox model proposed in Ref. [19] is considered in this work. The casing vibration signal

$$x(t) = FS_b \cdot x_b(t) + x_{dgd}(t) + x_n(t) + x_{imp}(t), \tag{10}$$

is decomposed in terms of a baseline bearing component $x_b(t)$; a bearing fault severity factor FS_b, which increases the magnitude of the bearing components; a damaged component attributed to distributed gear damage $x_{dgd}(t)$; a broadband noise component $x_n(t)$ and a bandlimited noise component $x_{imp}(t)$. The bandlimited noise or impulsive noise component is used to test the robustness of the FBI methods to the presence of spurious impulse components (i.e. impulsive information not related to the machine components of interest) and is only present for some clearly indicated measurements. Bandlimited impulses are for example expected for machines that operate in noisy environments, where impacts caused by nearby processes may excite the resonances of the gearbox under consideration or the resonances of nearby machines.

Detailed information regarding the different signal components, such as the signal-to-noise ratio can be found in Appendix B, with the important information highlighted here. The fundamental cyclic order of the BPOO is 4.12, while the fundamental cyclic order of the distributed gear damage component is 1.0 shaft order. The bearing component and the distributed gear damage components are centred in the spectrum at 7kHz and 1.3kHz, respectively. The distributed gear damage component is scaled to ensure that it is significantly more dominant than the bearing component for $FS_b = 1$ in the SES and therefore impedes the detection of the weak bearing component. The bandlimited noise component x_{imp} is centred at 12 kHz.

The simulated data are generated under time-varying speed conditions and constant load conditions. The rotational speed $\omega(t)$ is generated with a stochastic function, with samples from the function shown in Figure 3 to ensure that the speed of each generated signal is unique.

The casing vibration signal is presented in Figure 4 for two cases; the signal in Figure 4(i) is without the presence of the bandlimited impulses (i.e. $x_{imp}(t) = 0$ for $t \in \mathbb{R}$) and the signal in Figure 4(ii) contains the term $x_{imp}(t)$. The two bandlimited impulses are

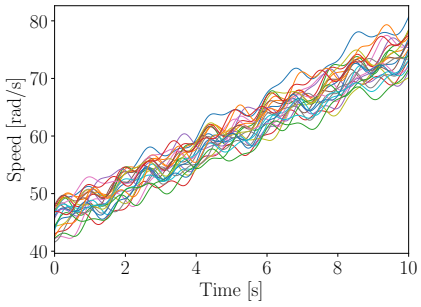

Figure 3: The rotational speed samples $\omega(t)$ that are used to generate the vibration data analysed in Section 3.

very prominent in Figure 4(ii) at 3 and 9 seconds respectively. The bandlimited impulsive

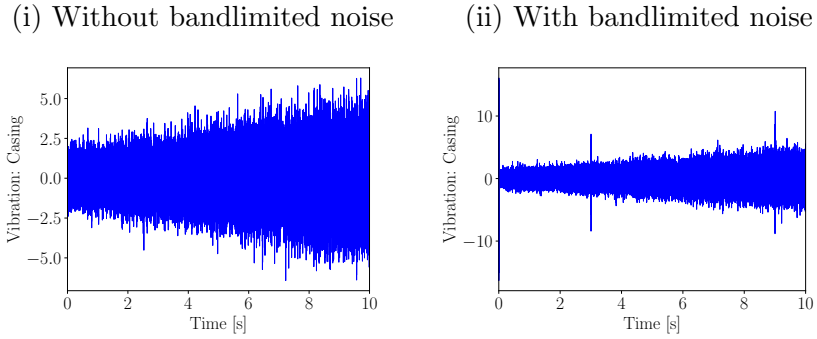

Figure 4: The casing vibration signal for the case without bandlimited noise added to the system (i.e. $x_{imp}(t) = 0$ for $t \in \mathbb{R}$) and for the case where bandlimited noise was added to the signal.

noise is not periodic, but introduces significant energy to a narrow frequency band around 12 kHz and therefore impedes the frequency band identification process.

Hence, the objective is to detect the weak bearing component in the presence of the dominant distributed gear damage component and the potential presence of impulsive noise, while the gearbox is operating under time-varying conditions.

3.2. Results with the IFBI$_\alpha$gram

The IFBI$_\alpha$gram proposed in Section 2 is investigated for the cases where bandlimited noise is either absent or present, and for two bearing fault severities, namely $FS_b = 1$ and $FS_b = 2$. For $FS_b = 2$, the bearing components are on average twice as large as the bearing components for $FS_b = 1$ under the same operating conditions. The aim is to determine the optimal frequency band for detecting the BPOO component and therefore $\{\alpha_f\} = \{4.12, 8.24, 12.36\}$ is used in Equation (3) to construct the feature planes.

The feature planes in Figure 5 are shown for the case where the bearing, the distributed gear damage and the noise components are generated from the same functions, but either without bandlimited noise or with bandlimited noise added to the signal. The identified

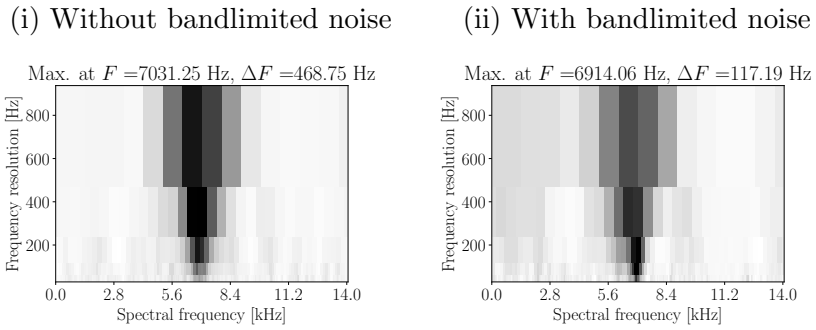

Figure 5: The casing vibration signal is shown for a bearing with a $FS_b = 1$ with the bandlimited impulsive noise term absent (see Figure 5(i)) or present (see Figure 5(ii)). The data are not presented on the same scales.

frequency bands (i.e. in the titles in Figures 5(i) and 5(ii)) are the frequency bands that maximise Equation (3) and takes into account the local signal-to-noise characteristics of the component-of-interest in the different frequency bands.

The feature planes in Figures 5(i) and 5(ii) look in principle the same; the IFBI$_\alpha$gram is not adversely affected by the presence of the bandlimited impulses or the distributed gear damage and identifies the frequency band at 7kHz correctly. The identified frequency bands are used to automatically design a bandpass filter for each signal, with the bandpass filtered signal compared to the raw signals in subsequent analyses.

The SES of the raw and filtered signals, with the latter obtained with the IFBI$_\alpha$gram, are shown in Figure 6 for the case without any bandlimited noise present in the signal, i.e. $x_{imp} = 0$ for $t \in \mathbb{R}$. The distributed gear damage component, located at 1 shaft order and its harmonics, dominates the SES of the raw signal in Figure 6(i) and masks the weak bearing component. However, by optimising the constructed feature plane to detect the cyclic orders of the BPOO and its two harmonics, it is possible to clearly detect the bearing component. The contributions of the distributed gear damage component can be completely removed with the bandpass filter, as seen in Figure 6(iii), because it does not manifest in the same spectral frequency band as the bearing.

In the case where $FS_b = 2$, the bearing component is significantly more prominent

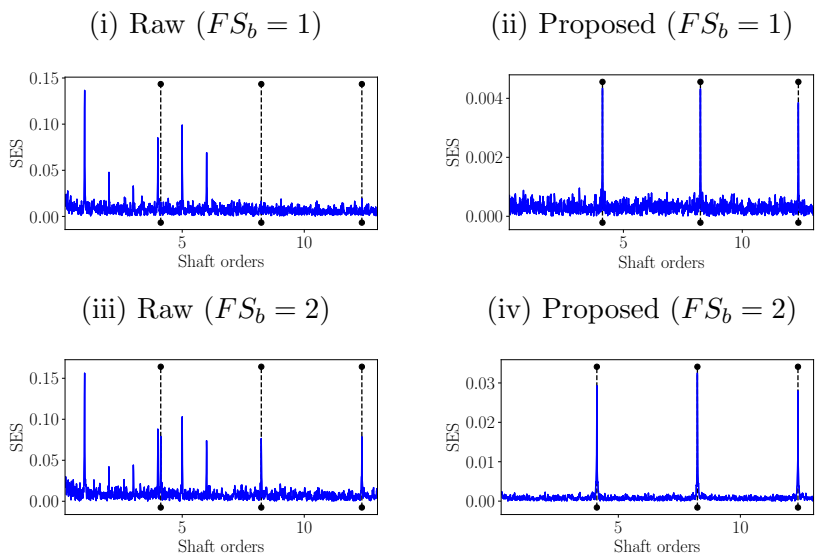

Figure 6: The Squared Envelope Spectra (SES) of the raw and filtered signals, with the latter obtained with the proposed method, are presented for two Fault Severity (FS) factors of the bearing. Bandlimited noise was not added to the signal.

in the SES of the raw signal and is not a challenge to detect. However, after applying the SES of the filtered signal in Figure 6(iv), the bearing component has a much better signal-to-noise ratio and is easier to interpret without the other interfering components.

The same analysis is performed for the case where the bandlimited noise component was present in the casing signal. The SES of these signals are shown in Figure 7. The raw signals in Figures 7(i) and 7(iii) have higher noise levels at the low-frequencies than the results in Figures 6(i) and 6(iii) due to the bandlimited impulses. However, the IFBI$_\alpha$gram is still able to extract the diagnostic information from the vibration signal and makes the bearing damage easy to detect as seen in Figure 7(ii) and 7(iv).

3.3. Results with the fast kurtogram

The fast kurtogram [27] is investigated on exactly the same datasets as in the previous section and is used to benchmark the IFBI$_\alpha$gram. The kurtogram is constructed by calculating the kurtosis of different bandlimited signals [27], i.e.

$$\mathcal{K}(f, \Delta f) = \frac{\left\langle |x(t, f; \Delta f)|^4 \right\rangle}{\left\langle |x(t, f; \Delta f)|^2 \right\rangle^2} - 2, \tag{11}$$

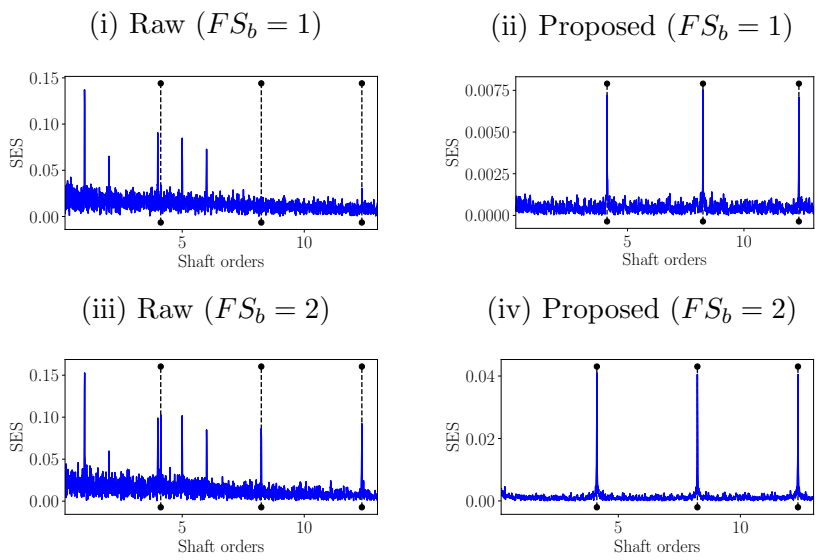

Figure 7: The Squared Envelope Spectra (SES) of the raw and filtered signals, with the latter obtained with the proposed method, are presented for two Fault Severity (FS) factors of the bearing. Bandlimited noise was added to the signal.

where the bandlimited signal associated with the band $[f - \Delta f/2, f + \Delta f/2]$ is denoted $x(t, f; \Delta f)$. The fast kurtogram performs the decomposition of the signal into the feature plane more efficiently, with a very fine grid being achieved as well.

The kurtogram is shown for the signals without bandlimited noise and with bandlimited noise in Figures 8(i) and 8(ii). In Figure 8(i), the kurtogram contains large values around the area of 1.3kHz, which indicates that the distributed gear damage component dominates the kurtogram, while the bearing component is not detected. However, if the

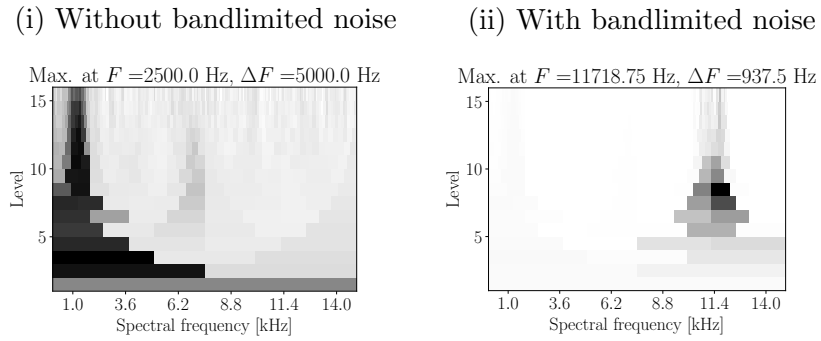

Figure 8: The fast kurtogram feature plane of the signal without bandlimited noise added to the casing signal is presented in Figure 8(i) and the kurtogram for the case where bandlimited noise was added to the casing signal is presented in Figure 8(ii). The data are not presented on the same scales.

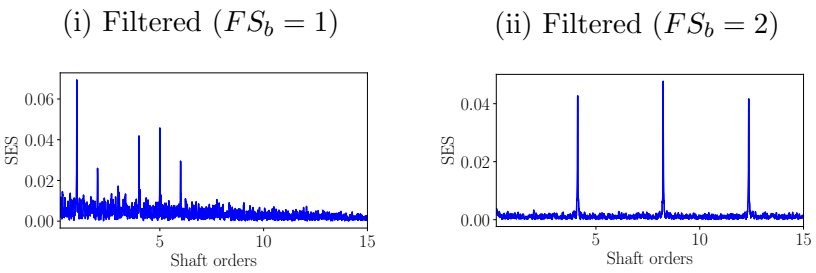

Figure 9: The Squared Envelope Spectra (SES) of the filtered signals, with the band determined with the fast kurtogram. Bandlimited impulsive noise was not added to the casing vibration signal.

bandlimited noise term, i.e. $x_{imp}(t)$, is non-zero in the casing vibration signal, the kurtogram is maximised by the bandlimited noise term, while both the gear and the bearing components remain undetected.

The SES of vibration signals without the bandlimited noise are investigated first with the results shown in Figure 9. The SES in Figure 9(i) corroborates the result in Figure 8(i); the distributed gear component dominates the kurtogram and is therefore very prominent in the filtered signal, while the weak bearing component remains undetected in the SES of the filtered signal.

If the magnitude of the bearing impulses are doubled, i.e. $FS_b = 2$, the bearing impulses dominate the kurtogram and is therefore present in the bandlimited signal as seen in Figure 9(ii). Hence, the kurtogram will only identify the frequency band of the bearing, if the impulses generated by the bearing damage have the most impulsiveness, i.e. if the damage is well developed.

However, if bandlimited impulsive noise $x_{imp}(t)$ is introduced in the signal, it is the most dominant component in the kurtogram as seen in Figure 8(ii). Therefore, the frequency band that is identified by the kurtogram is associated with the bandlimited impulsive noise. This influence of the bandlimited noise component on the SES is shown in Figure 10. The filtered signal does not contain any information related to the bearing and the distributed gear component, but only information related to the bandlimited impulse component.

3.4. Discussion: Kurtogram and IFBI$_\alpha$gram

Hence, in summary, the kurtogram identifies the frequency band with the most dominant kurtosis, irrespective of the periodicity of the component and most importantly the

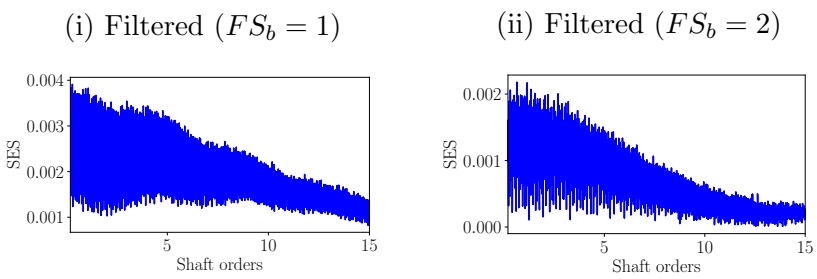

Figure 10: The Squared Envelope Spectra (SES) of the filtered signals, with the filtering band determined with the fast kurtogram. Bandlimited impulsive noise was added to the casing vibration signal.

machine component that generates the component. The FBI methods that use metrics based on the periodicity of the signal component, would only maximise the component that has the highest periodicity according to a criterion, e.g. sparsity or negentropy, and may not necessarily detect the incipient damage components. The IFBI$_\alpha$gram is robust to impulsive noise, but also allows us to optimise the detection of very specific cyclic components, as defined in the set $\{\alpha_f\}$.

In the next section, the IFBI$_\alpha$gram and the kurtogram are investigated on experimental gearbox data.

4. Experimental investigations

In this section, the IFBI$_\alpha$gram is compared to the kurtogram on experimental gearbox data. An overview of the experimental setup and a description of the data under consideration are given in Section 4.1, whereafter conventional analysis techniques are used to interrogate the data for the presence of damage in Section 4.2, the IFBI$_\alpha$gram is applied to the data in Section 4.3 and the kurtogram is applied to the data in Section 4.4. The purpose of this investigation is to show the following:

- The IFBI$_\alpha$gram works on experimental gearbox data acquired under time-varying operating conditions.
- The IFBI$_\alpha$gram can be used for gear damage detection, fault localisation and fault trending.
- The IFBI$_\alpha$gram can be combined with advanced signal analysis techniques such as the IES for fault detection.

4.1. Overview of experimental setup

The experimental data were acquired from a gearbox setup located in the Centre for Asset Integrity Management (C-AIM) laboratory at the University of Pretoria. The experimental gearbox setup, seen in Figure 11, consists of an electrical motor that drives the system, an alternator which dissipates the rotational energy, and three helical gearboxes. The centre helical gearbox is referred to as the test gearbox and is monitored for damage. Various sensors were placed on the test gearbox, with the axial component of a tri-axial

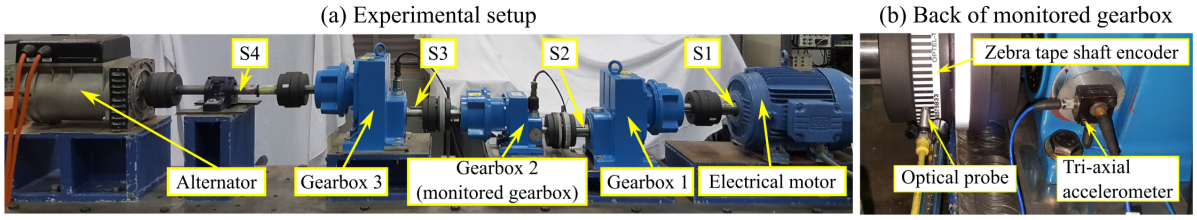

Figure 11: The experimental setup that was used to generate data in this work is presented with the important components highlighted. The tri-axial accelerometer, used to acquire the vibration data, and the optical probe, used to measure the tachometer signal, both located on the back of the gearbox, are also presented. S1, S2, S3, S4 refers to the four shafts of the system.

accelerometer, located on the back of the bearing casing of the test gearbox, used for monitoring. The rotational speed of the system is acquired from an optical probe and a zebra-tape shaft encoder. The geometrical imperfections of the zebra tape shaft encoder are attenuated by using a Bayesian geometrical compensation procedure [50]. All the data were acquired with an Oros OR35 data acquisition system. The accelerometer data were sampled at 25.6 kHz and the tachometer signal was sampled at 51.2 kHz.

The helical test gearbox contains a gear that rotates at 1.0 shaft order and a pinion that rotates at 1.85 shaft orders, with the shaft orders measured with respect to the input shaft of the gearbox on which the zebra tape shaft encoder is located (i.e. S2 in Figure 11(a)). A table of the different frequencies of the system is provided in Table 1.

Table 1: Normalised rotational speed and gear mesh frequencies of the system in Figure 11. All values were normalised with the speed of shaft $S2$.

	Gearbox 1	Gearbox 2	Gearbox 3
Rotational speed: Input	4.93	1.0	1.85
Rotational speed: Output	1.0	1.85	9.125
Meshing frequencies	74	37	136.9

The pinion was healthy for the duration of the test, but one of the teeth of the gear was seeded with damage as seen in Figure 12(i) before the experiment. The gearbox was operated with the operating conditions shown in Figure 13 for approximately 20 days whereafter the gear tooth failed. The gear with the missing tooth is shown in Figure 12(ii).

(i) Before (ii) After

Figure 12: The gear before the fatigue test with the seeded damage and the gear after the fatigue test are presented.

Twenty measurements, spaced evenly along the testing period was investigated to not only evaluate the ability of the IFBI$_\alpha$gram to extract diagnostic information for fault detection and fault localisation, but also show that it is possible to perform fault trending with the diagnostic metrics extracted from the filtered signals.

4.2. Conventional signal analysis techniques

The Power Spectral Density (PSD) and the Synchronous Average (SA) are investigated in this section to see whether it is possible to detect the gear damage in Figure 12 with conventional signal analysis techniques. The synchronous average is calculated with $N_0 =$

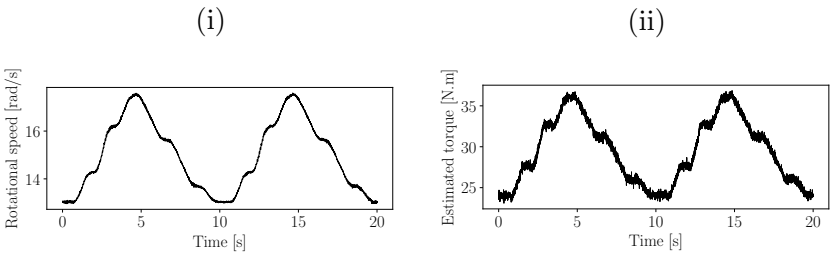

Figure 13: The speed and load that were present at the input shaft of the test gearbox during the measurements of the fatigue test.

46 for the gear and with $N_0 = 86$ for the pinion, where N_0 is the number of rotations used for averaging. The PSD and SA are presented in Figure 14 for two healthy and two damaged measurements. It is not possible to discern between the PSD of the healthy

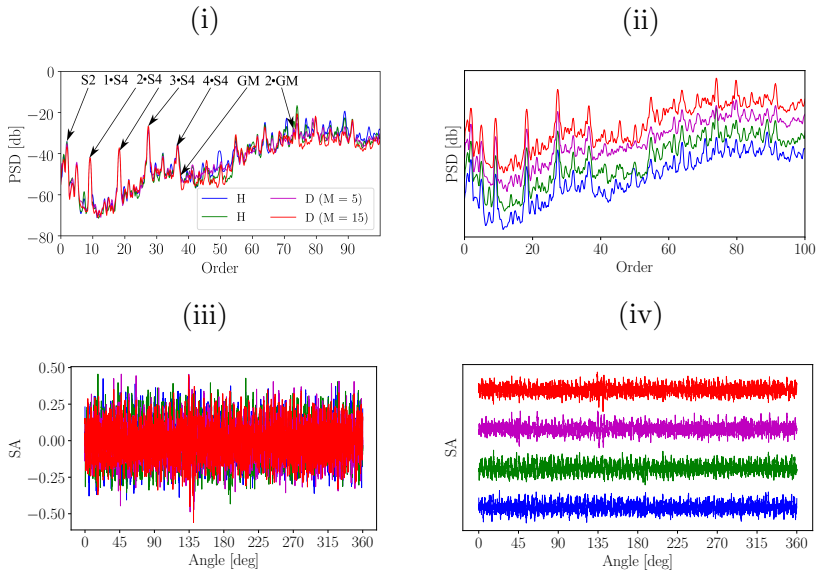

Figure 14: The Power Spectral Densities (PSD) and the Synchronous Average (SA) of the raw data are presented in Figures 14(i) and 14(iii) for two measurements. The label H means that the pinion and gear were healthy and $D(M = 15)$ indicates that it is the 15th measurement of the twenty measurements in the damaged dataset. The data are shifted in Figures 14(ii) and 14(iv) to make it easier to view the results. In Figure 14(i), the following abbreviations are used: S2: Shaft 2, S4: Shaft 2, GM: Gear Mesh. For the position of S2 and S4, see Figure 11.

and the damaged data in Figure 14(i). Even the gear mesh component at 37 orders and the shaft components of the damaged signals are approximately the same as the healthy signals. The SA performs slightly better than the PSD, with some indication of the damage

seen in Figure 14(iv) at approximately 135 degrees for the two damaged measurements. However, it is not very easy to detect the damage and the change in the condition of the gear between measurement 5 and 15 is not evident in Figure 14.

It is difficult to detect the gear damage with conventional methods as seen in Figure 12. This is attributed to the high noise levels and the fact that helical gears are used. The helical gears have high contact ratios and therefore when compared to spur gears, a smaller reduction in gear mesh stiffness is expected as a gear tooth deteriorates. Hence, conventional methods are ill-suited for diagnosing these gears and therefore it is necessary to use more sophisticated methods.

4.3. Proposed method

The gear and the pinion are monitored in this section to show that it is possible to discern between an healthy pinion and a gear with localised damage. Hence, for the gear, the feature in Equation (3) is calculated for the set $\{\alpha_f\} = \{1.0, 2.0, 3.0\}$ and for the pinion, the feature is calculated for the set $\{\alpha_f\} = \{1.85, 3.70, 5.55\}$.

The constructed feature planes are shown in Figure 15 for the gear and the pinion. The

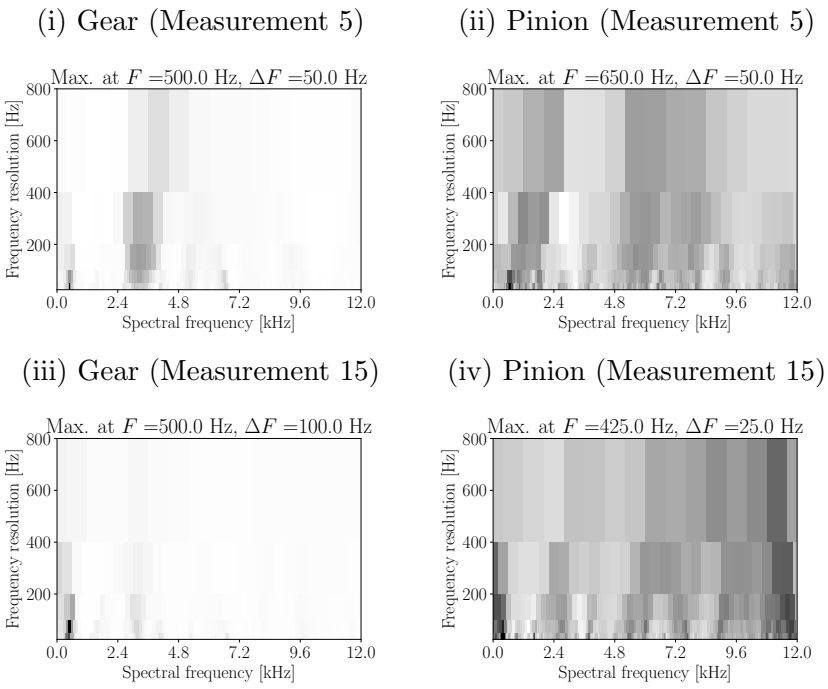

Figure 15: The feature planes that are obtained for the gear and the pinion with the IFBI$_\alpha$gram. The 5th and 15th measurements are under consideration. The data are not presented on the same scales.

large features of the gear are concentrated in a narrow resonance band at approximately 500Hz, while the feature plane of the pinion is much more uniform. The filtered signals for the gear and pinion are automatically calculated for the twenty measurements and analysed in subsequent sections. The filtered signal analyses are presented in the following sections: The Synchronous Average of the Squared Envelope (SASE) is investigated in Section 4.3.1, the Squared Envelope Spectrum (SES), the Enhanced Envelope Spectrum (EES) and the Improved Envelope Spectrum (IES) are investigated in Section 4.3.2 and the fault trending capabilities of the proposed method are investigated in Section 4.3.3.

4.3.1. Synchronous Average of the Squared Envelope (SASE)

The SASE of the raw and the SASE of the filtered signals are compared in Figure 16 for measurement number five of the twenty considered measurements. The filtered signals shown in this section was obtained by firstly calculating the IFBI$_\alpha$gram, then maximising it, whereafter the signal is filtered as shown in Figure 1. The SASE is calculated with

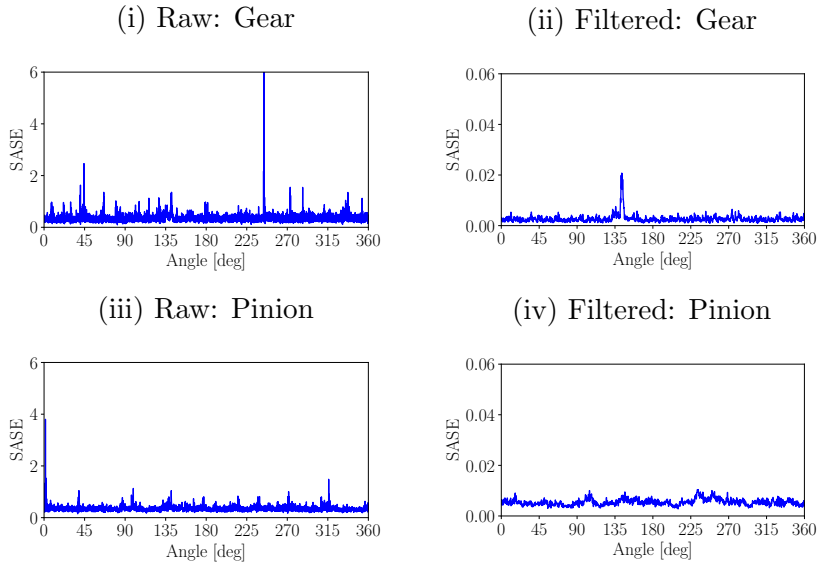

Figure 16: The Synchronous Average of the Square Envelope (SASE) is shown for the raw and the filtered signals, with the latter obtained with the proposed method. This was performed for measurement number 5 of the 20 measurements considered.

Equation (6), with either the order tracked raw signal or the order tracked filtered signal being used. The SASE of the gear was calculated by setting $\Phi_0 = 1$ and for the pinion $\Phi_0 = 0.541$. In Figure 16, the raw signals are dominated by the presence of spurious

impulses, i.e. they are not related to the condition of the gear, and therefore impede the condition monitoring process. However, the SASE of the filtered signals is much more intuitive; the gear contains prominent localised damage in the vicinity of 135 degrees, while the pinion is healthy.

The SASE of the raw and filtered signals are shown for measurement number 15 in Figure 17. The gear damage progressed from measurement 5 to 15 and therefore the

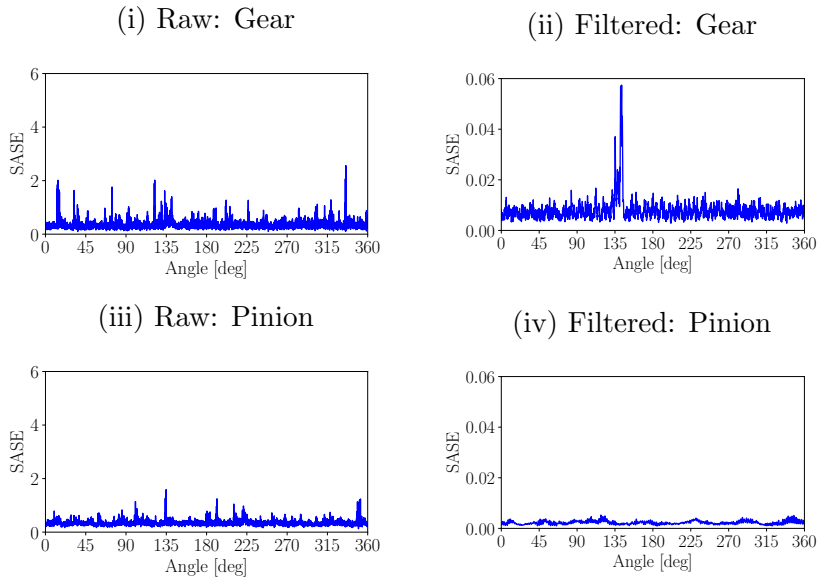

Figure 17: The Synchronous Average of the Squared Envelope (SASE) is shown of the raw and filtered signals, with the filtered signal obtained with the proposed method. This was performed for measurement number 15 of the 20 measurements considered.

damage is much more prominent in Figure 17(ii), while the pinion remains in healthy condition in Figure 17(iv). This is in contrast to the results of the raw signal, i.e. the SASE of the raw signal of the gears in Figure 17(i) and Figure 17(iii) are influenced by spurious impulses, which impedes the detection of the gear damage.

The slight fluctuations in the SASE of the pinion in Figures 16(iv) and 17(iv) are attributed to the non-synchronous impulses of the gear manifesting in the statistics of the pinion as well. However, it is clear from the results that the SASE can be used to visualise the condition of the gear, i.e. only a small portion of the gear is damaged.

4.3.2. Envelope spectra: SES, EES and IES

The SES is one of the most popular techniques for detecting periodicities in the instantaneous power of the signal and the damaged gear components would manifest at 1.0 shaft order and a damaged pinion component would manifest at 1.85 shaft orders. The SES of the raw and filtered signals are shown in Figure 18 for measurement number 5. The raw signal does not reveal any signal components related to the gear nor the pinion, while there are other signal components which impede the interpretation of the results. The impulses that impeded the SASE of the raw signals, manifest at 5.72 shaft orders. In contrast, the proposed method performs exceptionally well in extracting the damaged

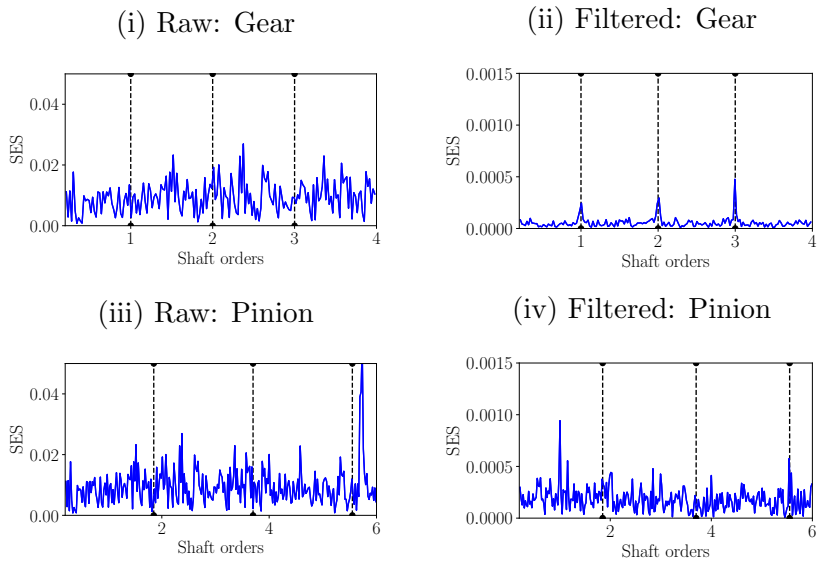

Figure 18: The Squared Envelope Spectra (SES) of the raw and filtered signals that were obtained with the proposed method. The SES of the filtered signal, obtained by maximising for the gear and pinion, are shown in Figures 18(ii) and 18(iv), respectively. The results are shown for measurement number 5 of the 20 considered.

components and therefore the signal components attributed to the gear damage are clearly seen in the filtered signals, while the pinion does not provide strong evidence that it is damaged.

The SES of the second signal, measurement number 15, is shown in Figure 19 for the raw and filtered signals. The SES of the raw signals still do not contain any clear diagnostic information and therefore cannot be used to infer the condition of the gears. However, the gear components are even larger in the SES of the filtered when compared

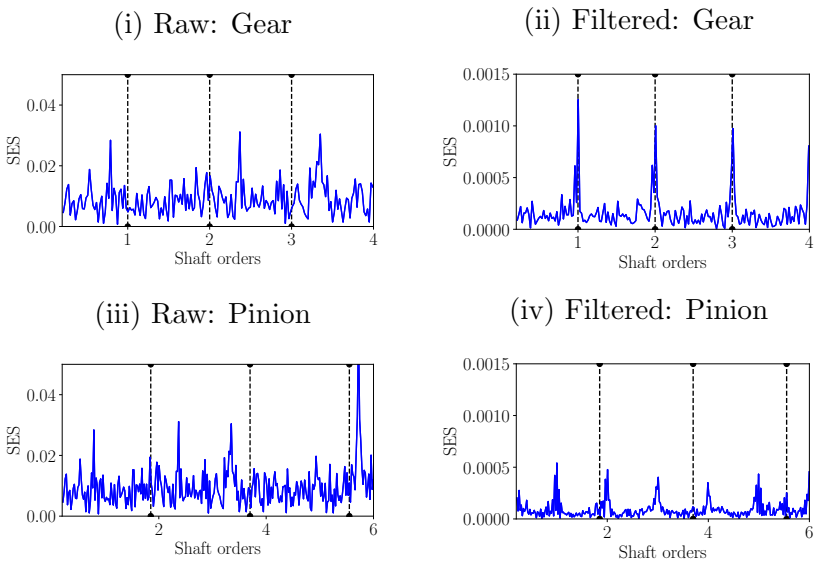

Figure 19: The SES of the raw and filtered signals, with the latter obtained with the proposed method, are shown for measurement number 15 of the 20 considered.

to Figure 19, i.e. a change in condition is evident.

A very interesting result is observed in the SES of the filtered signal for the pinion shown in Figure 19(iv). There are no clear pinion components located at 1.85 shaft orders, which indicates that the pinion is healthy. However, the dominant components at 1.0 shaft order and its harmonics indicate that the filtered signal contains information related to the gear as well. This emphasises that the filtered signal is optimal to detect specific cyclic orders, but might not be independent of other damage modes and therefore care should be taken when using statistics such as the RMS or kurtosis of the filtered signals to infer the conditions of specific components.

The EES and the IES, calculated with Equations (8) and (9) respectively, are presented in Figure 20 for the same measurements as the SES investigations. However, instead of calculating the OFSCoh of the raw signal, the OFSCoh was calculated with a signal that was whitened with the CPW procedure as discussed in Ref. [16]. This is to further emphasise that signal enhancing tools can be used with the IFBI$_\alpha$gram. The IES is calculated with the frequency band that is estimated with the IFBI$_\alpha$gram for the gear, i.e. $\{\alpha_f\} = \{1.0, 2.0, 3.0\}$. The EES of the two measurements do not contain any information related to the component of the gear, while being rich with other signal components. In contrast, the IES is very rich with diagnostic information pertaining to the gear with very

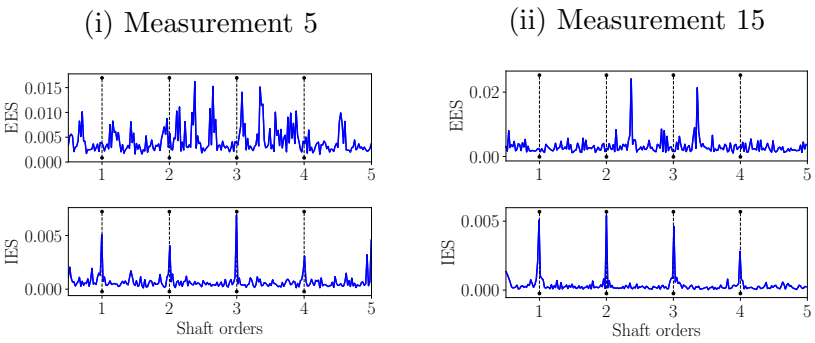

Figure 20: The Enhanced Envelope Spectrum (EES) and the Improved Envelope Spectrum (IES) are shown for measurements 5 and 15. The Improved Envelope Spectra are calculated by using the frequency bands that were identified by the IFBI$_\alpha$gram for the gear.

distinct harmonics seen at a shaft order of 1 and its harmonics. Therefore, the IFBI$_\alpha$gram can be used to calculate the IES for detecting very specific damage components.

4.3.3. Fault trending

Even though it is extremely important to detect faults early, it is equally very important to be able to detect changes in the condition of the components. Therefore, in this section, the suitability of the filtered signal for fault trending is investigated. The SASE of the raw and the filtered signals are presented in Figure 21 over the twenty measurements to visualise the deterioration of the gear. The noise in Figure 21(i) is dominant and impedes the ability to infer the condition of the gear and it also makes it difficult to observe changes in the condition of the gear.

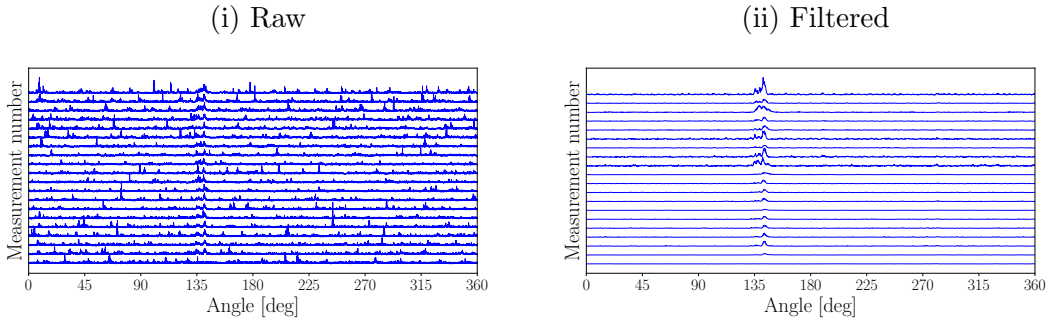

Figure 21: The Synchronous Averages of the Squared Envelope (SASE) of the raw and the filtered signals are shown for the twenty measurements considered.

The filtered signal in Figure 21(ii) performs significantly better than the raw signal in

Figure 21(i). The SASE contains only information related to the gear component, with the gear damage and the increasing severity of the damage easily seen.

The benefits of using the IFBI$_\alpha$gram are further emphasised by the results in Figure 22 as well. The SES of the raw signals in Figure 22(i) do not contain any clear diagnostic information pertaining to the gear, while the 1.0 shaft order component and its harmonics are clearly seen in the SES of the filtered signal in Figure 22(ii).

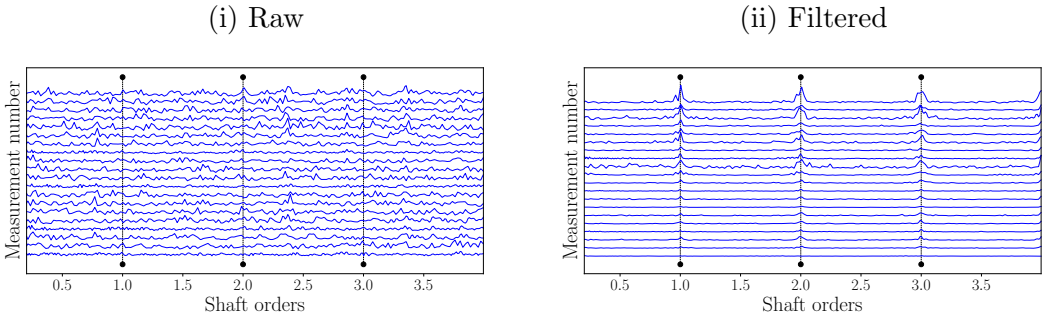

Figure 22: The Squared Envelope Spectra (SES) of the raw and the processed signals, obtained with the proposed method by using the cyclic order set of the gear, are shown for the twenty measurement numbers.

Usually in condition monitoring, a one-dimensional metric such as the RMS or the kurtosis is utilised for change detection. However, the kurtosis and RMS can lead to misleading results when determining changes in specific mechanical components. The feature calculated with Equation (4) can be used on the SES with a similar procedure as Ref. [41] for fault trending. This means that $\sum_{\alpha\in\{\alpha_f\}} \mathrm{SNR}\left\{\mathrm{SES}_{\boldsymbol{x}}\left(\alpha\right)\right\}$, is calculated to detect changes in the signal-to-noise ratio of specific components in the SES. This metric is calculated for the raw and filtered signals and is presented in Figure 23.

The metrics of the raw signals of the gear and the pinion remain approximately constant for all measurements, which erroneously indicates that the gear and pinion are both in a healthy condition. However, when investigating the metrics of the filtered signals, it can be observed that the metric of the gear actually changes considerably over time, while remaining constant for the pinion. Therefore, by combining the metric in Equation (4) with the SES of the filtered signal, it is possible to separately detect changes in the condition of the gear and the pinion. This is important for large gearboxes such as applications where girth gears and pinions are separately ordered.

(i) Gear (ii) Pinion

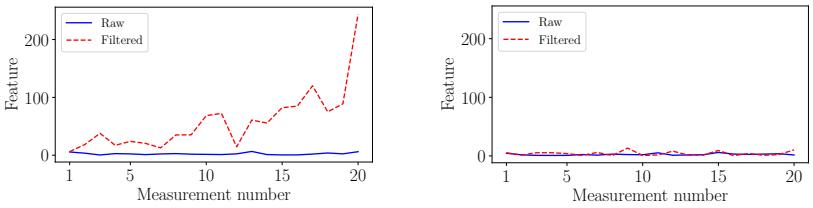

Figure 23: The fault trending metrics, which combines Equation (4) with the SES, are presented for the raw and filtered signals. The metric for the gear is calculated with $\{\alpha_f\} = \{1.0, 2.0, 3.0\}$, and the metric for the pinion is calculated with $\{\alpha_f\} = \{1.85, 3.70, 5.55\}$.

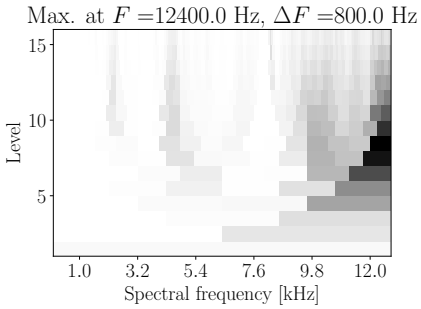

Figure 24: The feature plane, obtained with the fast kurtogram, is shown for measurement number 15.

4.4. Fast kurtogram

The fast kurtogram is investigated on the same data as the previous section to further illustrate the benefits of using the IFBI$_\alpha$gram. The kurtogram is shown in Figure 24 for the same signal investigated in Figure 15. The repetitive transients, which adversely affected the SASE and SES results in the raw signal, manifest in the higher frequency bands and dominate the kurtogram. Even though these repetitive transients are cyclostationary, they are not associated with the specific components under consideration, and therefore impedes detecting the damaged gear components.

The adverse influence of the repetitive transients are further seen in Figure 25, where the SASE and SES of the filtered signals are presented over all the measurements. The limited diagnostic information in the SASE of the raw signal, presented in Figure 21(i), is completely removed by the kurtogram as seen in Figure 25(i). The SES indicates that the impulsive information seen in the SASE and identified by the kurtogram is attributed to the repetitive transients which have a fundamental cyclic order of 5.72.

Lastly, similarly to the previous section, the fault trending capabilities of the feature

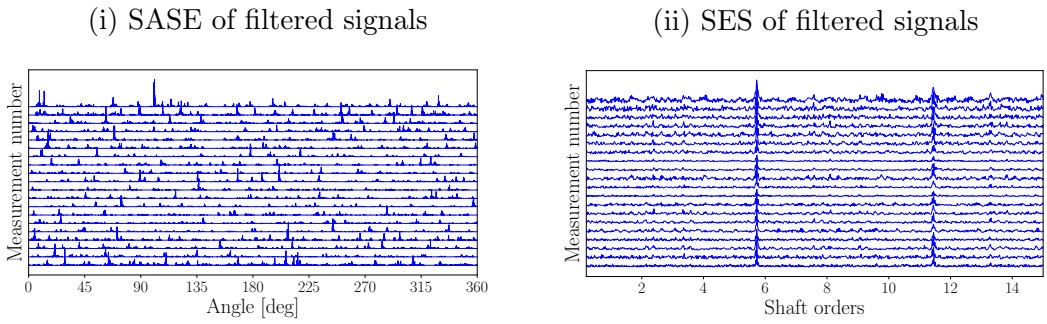

Figure 25: The Synchronous Averages of the Squared Envelope (SASE) and the Squared Envelope Spectra (SES) of the filtered signals are presented for the measurements considered.

in Equation (4), calculated for the SES of raw and filtered signals, are investigated and shown in Figure 26 for the gear. Since the filtered signal only contains information related

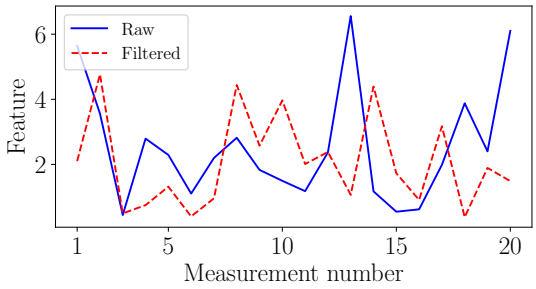

Figure 26: The feature, defined by Equation (4), is calculated with the SES for the cyclic orders associated with the gears.

to the repetitive transients at 5.72 orders, the feature presented in Figure 26 does not contain any changes in the gear component. Hence, the kurtogram is adversely affected by the presence of the repetitive transients not related to the gearbox, which results in the gear damage and the gear failure to be undetected.

4.5. ICS2gram

The ICS2gram is another method that can be used to search for frequency bands related to a set of cyclic orders $\alpha \in \{\alpha_f\}$ [38, 42]. The feature [38, 42]

$$\mathrm{ICS2}(f, \Delta f; \{\alpha_f\}) = \sum_{\alpha \in \{\alpha_f\}} \frac{|\mathrm{SES}(\alpha; f, \Delta f)|^2}{|\mathrm{SES}(0; f, \Delta f)|^2}, \tag{12}$$

is calculated from the Squared Envelope Spectrum (SES) of the bandlimited signal denoted $x(t; f, \Delta f)$. In the paper by Smith et al. [42], the averaged speed was used to calculate

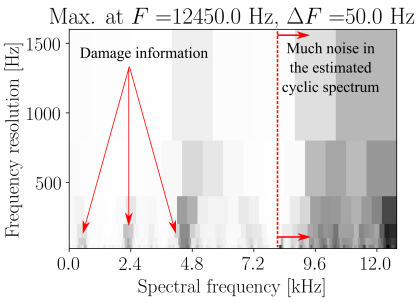

Figure 27: The feature plane, obtained with the ICS2gram, is presented for the case where $\{\alpha_f\} = \{1.0, 2.0, 3.0\}$.

the ICS2gram based on frequency-frequency representation of the signal. However, this is a poor approximation under time-varying speed conditions and therefore to ensure that a fair comparison is made, the authors compared the proposed method against the Order-Frequency based ICS2gram. This is estimated by firstly calculating the Order-Frequency Cyclic Modulation Spectrum (OFCMS) [14], which is used to estimate the SES of different spectral frequency bands, whereafter Equation (12) was applied on each frequency band separately. The motivation behind using the OFCMS is to ensure that the feature is consistent under time-varying speed conditions and the comparison with the proposed IFBI$_\alpha$gram is fair.

The motivation behind this investigation is to further emphasise the benefits of the proposed method. The resulting feature plane obtained for only the damaged gear is shown in Figure 27 for measurement 15, which is also considered in Figures 15 and 24. The 500 Hz frequency band seen in Figure 15 is also prominent in the ICS2gram, however, the ICS2gram is dominated by the noise in the higher frequency bands clearly highlighted in Figure 27. This results in the wrong frequency bands to be identified in the signal.

The SES and the SASE of the resulted filtered signals are shown in Figure 28, for the same signals shown in Figure 21, 22 and 25. It is evident from the SASE and SES identified by the ICS2gram that the wrong frequency band was detected for most cases. This is attributed to the noise in the estimated cyclic spectra of the high spectral frequency bands. Hence, the proposed IFBI$_\alpha$gram performs much better than the kurtogram and the ICS2gram on the detecting the gear damage in this dataset.

It is possible that if the log-envelope spectrum is investigated instead of the SES, the

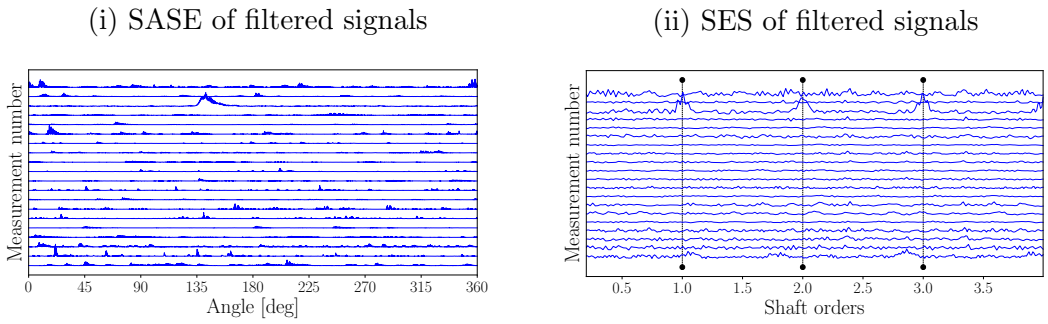

Figure 28: The Synchronous Averages of the Squared Envelope (SASE) and the Squared Envelope Spectra (SES) of the filtered signals, obtained with the ICS2gram, are presented for the measurements considered.

ICS2gram would be more robust to non-Gaussian noise. However, the log of the OFSCoh can also be used in the calculation of the IFBI$_\alpha$gram and therefore for the purposes of this comparison it is not investigated. It is therefore clear that the new proposed feature, discussed in Section 2.2, has much potential for detecting components-of-interest.

4.6. Calculation time of the IFBI$_\alpha$gram

Most of the calculation time of the IFBI$_\alpha$gram is attributed to the calculation of the spectral correlation for the set of spectral coherences in Figure 1. The computational time is dependent on the estimator, the considered cyclic order ranges and the cyclic order resolution that is required. In this work, the spectral correlation is estimated with a Welch estimator due to its good bias and variance properties. The average calculation time of different spectral coherences are given in Table 2 for the experimental data in Section 4.1.

Table 2: The average calculation time of the spectral coherence with a Welch estimator, for a single α but all frequencies f, are presented as a function of window length N_w for the experimental gearbox data. The vibration data contained on average 496000 samples and were sampled at 25.6 kHz. The functions are implemented in Python 3.5.4 on a computer with an Intel Core i7 2.50 GHz CPU and 16 GB of RAM.

N_w	16	32	64	128	256	512
Time [s]	15.30	7.73	4.58	2.55	1.73	1.27

This resulted in the calculation of the IFBI$_\alpha$gram for both gears to be approximately 2.5 hours for the window lengths in Table 2. However, the computational time of the

IFBI$_\alpha$gram can be significantly improved if the code is optimised and if more computational efficient methods such as the cyclic modulation spectrum [14] or the fast and faster spectral correlation estimators [45, 46] are used. For example, if the asymptotic results in Ref. [45] are used, then the computational gain of the fast spectral correlation over the Welch estimator is $L/(2 \cdot R)$, where L is the signal length and R is the block shift in the short-time Fourier transform. This means that the computational time of each spectral correlation can theoretically be reduced by a factor between 968 and 15489 for the data in Table 2 when using the fast spectral correlation instead of the Welch estimator. These estimators will be used to calculate the IFBI$_\alpha$gram in future investigations.

5. Conclusions

In this work, the IFBI$_\alpha$gram is proposed for automatically identifying frequency bands that are rich with diagnostic information pertaining to specific mechanical components under time-varying operating conditions. By identifying these frequency bands and using this information with sophisticated signal analysis techniques, it is possible to detect weak signal components due to incipient damage on the components-of-interest. The IFBI$_\alpha$gram is compared to the kurtogram on numerical and experimental data, where it is shown that the IFBI$_\alpha$gram allows the following:

- Incipient damage detection, identification of the damaged components and detection of changes in the condition of different components.
- Identification of optimal bands for detecting weak components can be determined despite the presence of other dominating components such as impulsive noise or more severely damaged components.
- Effective condition monitoring under time-varying operating conditions.

Ultimately, the success of this method is ascribed to the SNR feature that is used on each spectral frequency band of the order-frequency spectral coherence. The spectral coherence is capable of highlighting weak components in the signal under time-varying operating conditions and it does not suffer from the same limitations as time-frequency based cyclic spectrum estimators; while the signal-to-noise ratio feature is capable of finding spectral

frequency bands were the component-of-interest is most prominent in the cyclic spectrum. This has the additional benefit that this feature is robust to high noise levels in the cyclic spectrum.

Acknowledgements

The South African authors gratefully acknowledge the support that was received from the Eskom Power Plant Engineering Institute (EPPEI).

Appendix A. Motivation for the median

In Equation (4), the amplitude of the signal component is divided by the estimated noise level to measure the signal-to-noise ratio of specific components in a spectrum. The noise level in the spectrum at a specific cyclic order α needs to be estimated from the data. In Section 2.2, it is proposed that the data in the band $\alpha \in [\alpha_f - 1, \alpha_f + 1]$ can be used to estimate the noise level at α_f. Different signal components may be present in this cyclic order band, which can result in the noise level to be overestimated when using a metric that is sensitive to these harmonics. Also, if the band is chosen too small (to minimise the number of signal components in this band), then too few data points might be available to properly estimate the noise level. Hence, the suitability of the average, median and Root-Mean-Square (RMS) to estimate the noise level is investigated on a synthetic dataset where the noise level is known.

A synthetic signal

$$y(t) = \kappa \cdot x(t) + n(t), \tag{A.1}$$

is used to compare the performance of the considered metrics, where κ is a factor which increases the contribution of the deterministic function $x(t)$ and $n(t)$ is Gaussian noise. The function

$$x(t) = \sum_{k=1}^{N} \sin(2 \cdot \pi \cdot t \cdot f_0 \cdot k), \tag{A.2}$$

is used to generate the deterministic function, where $N = 20$ and $f_0 = 100$ Hz. The power spectral density of the signal $y(t)$, denoted $P_y(f)$ and the power spectral density of the noise $n(t)$, denoted $P_n(f)$ are used to compare the suitability of three metrics, namely the average, the median and the RMS to estimate the noise level of n from y.

The performance of the each metric is quantified with the Logarithm of the Absolute Difference (LAD)

$$\text{LAD} = \log |\mathcal{S}(P_y(f)) - \mathcal{S}(P_n(f))|, \tag{A.3}$$

between the metric $\mathcal{S}$ (e.g. median) of the power spectral density of y, denoted P_y and the metric $\mathcal{S}$ of the power spectral density of n, denoted P_n for different κ. If the LAD is small, it indicates that the metric $\mathcal{S}$ is able to estimate the noise level accurately from the full signal y and is independent of the signal components $\kappa \cdot x(t)$.

The results are shown in Figure A.29 for the three considered metrics. It can be seen

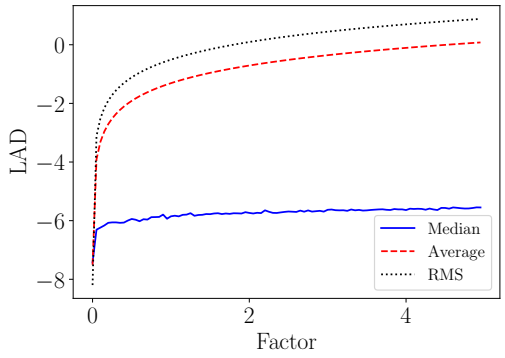

Figure A.29: The Logarithm of the Absolute Difference (LAD) between a metric of the PSD of signal y and the metric of the PSD of the signal n.

that the average and the RMS are only able to estimate the noise level well for very small κ, i.e. when the contribution of $\kappa \cdot x(t)$ is negligible in Equation (A.1). This means that the average and the RMS are sensitive to the presence of signal components in the frequency band that is used to estimate the noise level.

In contrast to the average and RMS, the median is very insensitive to the magnitude of κ. This indicates that the median is unaffected by the signal components and can therefore be used to obtain a more reliable estimate of noise level. Hence, the median is used in this work to estimate $\mathcal{G}$ in Equation (4).

Appendix B. Numerical gearbox model

The casing vibration signal in Equation (10) can be decomposed in terms of a distributed gear damage component, a bearing component, a broadband noise component

and a filtered noise component. An overview of each component is given in this section, but more information can be found in [19].

The distributed gear damage component

$$x_{dgd}(t) = M\left(\omega(t)\right) \cdot h_{dgd}(t) \otimes \left(\epsilon_n(t) \cdot \sum_{k=1}^{N_{dgd}} A_k^{dgd} \sin\left(\theta(t) \cdot k + \phi_k^{dgd}\right) \right), \tag{B.1}$$

where $\epsilon_n(t)$ is sampled from a zero-mean Gaussian distribution with a unit variance, $\theta(t) = \int_0^t \omega(\tau) d\tau$ is the instantaneous phase of the shaft, $M\left(\omega\right) = \omega^2$ simulates the dependence of the amplitude of the signal to speed, and h_{dgd} is a single degree-of-freedom impulse response function with a natural frequency of 1300 Hz and a damping ratio of 0.05. There are N_{dgd} harmonics of the distributed gear damage component in the signal, with the amplitude and phase of the kth harmonic denoted A_k^{dgd} and ϕ_k^{dgd} respectively.

The baseline bearing component

$$x_b(t) = M(\omega(t)) \cdot h_b(t) \otimes \left(\sum_{k=1}^{N_b} \delta\left(t - T_k\right) \right), \tag{B.2}$$

consists of the same modulation function $M(t)$ as the distributed gear damage component. The single degree-of-freedom impulse response function h_b has a damping ratio of 0.05 and a natural frequency of 7.0 kHz. The Dirac function $\delta(t) = 1$ if $t = 0$ and 0 otherwise. The time-of-arrival of the kth bearing impulse T_k is a function of the instantaneous phase of the shaft, the geometry of the bearings as well as slippage effects [11, 19].

The broadband noise component

$$x_n(t) = M(\omega(t)) \cdot \epsilon_n(t), \tag{B.3}$$

consists of a zero-mean Gaussian noise component $\epsilon_n(t)$ with a unit variance and the influence of speed on the noise level $M(\omega) = \omega^2$.

Lastly, the bandlimited signal component

$$x_{imp}(t) = h_{imp}(t) \otimes \left(\epsilon(t; 3, 3.01) + \epsilon(t; 9, 9.01)\right), \tag{B.4}$$

consists of a bandpass impulse response function that passes the frequency content between 10.5 kHz and 13.5 kHz and two functions in the form of $\epsilon(t; t_1, t_2)$. The function $\epsilon(t; t_1, t_2)$ contains zero-mean Gaussian noise for $t \in [t_1, t_2]$ and is zero otherwise. This signal is only included in the casing signal for some of the datasets, as clearly highlighted in the results.

The casing vibration signal is shown with the distributed gear damage component, the bearing component and the rotational speed component in Figure B.30. The dependence of the amplitude of the signals to changes in speed, is evident in the results.

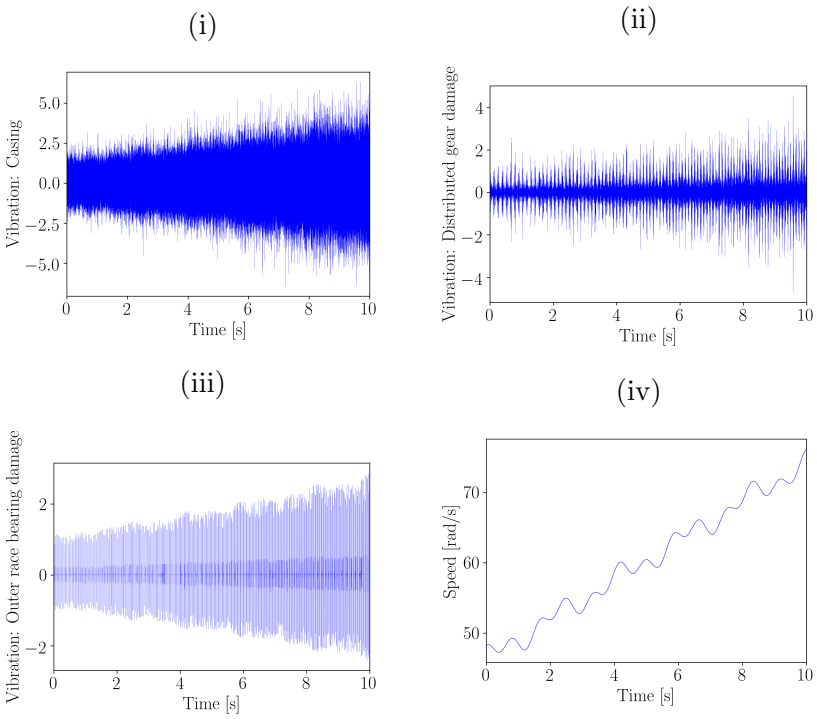

Figure B.30: The casing vibration signal, distributed gear damage component, the bearing component and the rotational speed of the input shaft of the gearbox are presented for a $FS_b = 1$.

Some statistics of the casing vibration signal and its components are given in Table B.3.

Table B.3: The statistics of the different signal components are shown for $FS_b = 1$. The SNR_{db} is defined as $10 \cdot \log_{10}(E_i/E_n)$ where E_i is the energy of signal component i and E_n is the energy of the noise component.

Statistics	x_c	x_{dgd}	x_b	x_n	x_{imp}
Kurtosis	3.556	6.716	95.236	0.667	1500.236
RMS	1.402	0.925	0.150	1.008	0.263
SNR_{db}	-	-0.748	-16.574	0	-11.684

References

[1] J. P. Salameh, S. Cauet, E. Etien, A. Sakout, L. Rambault, Gearbox condition monitoring in wind turbines: A review, Mechanical Systems and Signal Processing 111 (2018) 251–264.

[2] A. Mauricio, K. Gryllias, S. Sheng, Condition monitoring of wind turbine planetary gearboxes under different operating conditions, in: Proceedings of ASME Turbo Expo 2019 Turbomachinery Technical Conference and Exposition, ASME.

[3] L. Saidi, J. B. Ali, E. Bechhoefer, M. Benbouzid, Wind turbine high-speed shaft bearings health prognosis through a spectral kurtosis-derived indices and svr, Applied Acoustics 120 (2017) 1–8.

[4] P. D. Samuel, D. J. Pines, A review of vibration-based techniques for helicopter transmission diagnostics, Journal of Sound and Vibration 282 (2005) 475–508.

[5] A. Mauricio, L. Zhou, D. Mba, K. Gryllias, Vibration based condition monitoring of helicopter gearboxes based on cyclostationary analysis, in: Proceedings of ASME Turbo Expo 2019 Turbomachinery Technical Conference and Exposition, ASME.

[6] C. J. Stander, P. S. Heyns, W. Schoombie, Using vibration monitoring for local fault detection on gears operating under fluctuating load conditions, Mechanical Systems and Signal Processing 16 (6) (2002) 1005–1024.

[7] W. Bartelmus, R. Zimroz, Vibration condition monitoring of planetary gearbox under varying external load, Mechanical Systems and Signal Processing 23 (1) (2009) 246–257.

[8] R. Zimroz, W. Bartelmus, T. Barszcz, J. Urbanek, Diagnostics of bearings in presence of strong operating conditions non-stationarity - A procedure of load-dependent features processing with application to wind turbine bearings, Mechanical Systems and Signal Processing 46 (1) (2014) 16–27.

[9] J. Antoni, F. Bonnardot, A. Raad, M. El Badaoui, Cyclostationary modelling of

rotating machine vibration signals, Mechanical Systems and Signal Processing 18 (6) (2004) 1285–1314.

[10] R. B. Randall, J. Antoni, Rolling element bearing diagnostics-A tutorial, Mechanical Systems and Signal Processing 25 (2) (2011) 485–520.

[11] D. Abboud, J. Antoni, M. Eltabach, S. Sieg-Zieba, Angle\time cyclostationarity for the analysis of rolling element bearing vibrations, Measurement 75 (2015) 29–39.

[12] S. Baudin, D. Rémond, J. Antoni, O. Sauvage, Non-intrusive rattle noise detection in non-stationary conditions by an angle/time cyclostationary approach, Journal of Sound and Vibration 366 (2016) 501–513.

[13] D. Abboud, S. Baudin, J. Antoni, D. Rémond, M. Eltabach, O. Sauvage, The spectral analysis of cyclo-non-stationary signals, Mechanical Systems and Signal Processing 75 (2016) 280–300.

[14] D. Abboud, J. Antoni, Order-frequency analysis of machine signals, Mechanical Systems and Signal Processing 87 (2017) 229–258.

[15] D. Abboud, J. Antoni, S. Sieg-Zieba, M. Eltabach, Deterministic-random separation in nonstationary regime, Journal of Sound and Vibration 362 (2016) 305–326.

[16] P. Borghesani, P. Pennacchi, R. B. Randall, N. Sawalhi, R. Ricci, Application of cepstrum pre-whitening for the diagnosis of bearing faults under variable speed conditions, Mechanical Systems and Signal Processing 36 (2) (2013) 370–384.

[17] W. Wang, Early detection of gear tooth cracking using the resonance demodulation technique, Mechanical Systems and Signal Processing 15 (5) (2001) 887–903.

[18] P. McFadden, M. Toozhy, Application of synchronous averaging to vibration monitoring of rolling element bearings, Mechanical Systems and Signal Processing 14 (6) (2000) 891–906.

[19] D. Abboud, J. Antoni, S. Sieg-Zieba, M. Eltabach, Envelope analysis of rotating machine vibrations in variable speed conditions: A comprehensive treatment, Mechanical Systems and Signal Processing 84 (2017) 200–226.

[20] J. Cheng, Y. Yang, D. Yu, The envelope order spectrum based on generalized demodulation time–frequency analysis and its application to gear fault diagnosis, Mechanical Systems and Signal processing 24 (2) (2010) 508–521.

[21] J. Urbanek, T. Barszcz, R. Zimroz, J. Antoni, Application of averaged instantaneous power spectrum for diagnostics of machinery operating under non-stationary operational conditions, Measurement 45 (7) (2012) 1782–1791.

[22] Z. Peng, F. Chu, Application of the wavelet transform in machine condition monitoring and fault diagnostics: a review with bibliography, Mechanical systems and signal processing 18 (2) (2004) 199–221.

[23] Y. Lei, J. Lin, Z. He, M. J. Zuo, A review on empirical mode decomposition in fault diagnosis of rotating machinery, Mechanical systems and signal processing 35 (1-2) (2013) 108–126.

[24] J. Antoni, R. B. Randall, The spectral kurtosis: Application to the vibratory surveillance and diagnostics of rotating machines, Mechanical Systems and Signal Processing 20 (2) (2006) 308–331.

[25] J. Antoni, The spectral kurtosis: A useful tool for characterising non-stationary signals, Mechanical Systems and Signal Processing 20 (2) (2006) 282–307.

[26] F. Combet, L. Gelman, Optimal filtering of gear signals for early damage detection based on the spectral kurtosis, Mechanical Systems and Signal Processing 23 (3) (2009) 652–668.

[27] J. Antoni, Fast computation of the kurtogram for the detection of transient faults, Mechanical Systems and Signal Processing 21 (1) (2007) 108–124.

[28] T. Barszcz, R. B. Randall, Application of spectral kurtosis for detection of a tooth crack in the planetary gear of a wind turbine, Mechanical Systems and Signal Processing 23 (4) (2009) 1352–1365.

[29] J. Antoni, The infogram: Entropic evidence of the signature of repetitive transients, Mechanical Systems and Signal Processing 74 (2016) 73–94.

[30] T. Barszcz, A. Jabłoński, A novel method for the optimal band selection for vibration signal demodulation and comparison with the kurtogram, Mechanical Systems and Signal Processing 25 (1) (2011) 431–451.

[31] D. Wang, P. W. Tse, K. L. Tsui, An enhanced kurtogram method for fault diagnosis of rolling element bearings, Mechanical Systems and Signal Processing 35 (1-2) (2013) 176–199.

[32] P. W. Tse, D. Wang, The design of a new sparsogram for fast bearing fault diagnosis: Part 1 of the two related manuscripts that have a joint title as "two automatic vibration-based fault diagnostic methods using the novel sparsity measurement - Parts 1 and 2", Mechanical Systems and Signal Processing 40 (2) (2013) 499–519.

[33] W. A. Smith, Z. Fan, Z. Peng, H. Li, R. B. Randall, Optimised spectral kurtosis for bearing diagnostics under electromagnetic interference, Mechanical Systems and Signal Processing 75 (2015) 371–394.

[34] D. Wang, An extension of the infograms to novel Bayesian inference for bearing fault feature identification, Mechanical Systems and Signal Processing 80 (2016) 19–30.

[35] X. Xu, M. Zhao, J. Lin, Y. Lei, Envelope harmonic-to-noise ratio for periodic impulses detection and its application to bearing diagnosis, Measurement 91 (2016) 385–397.

[36] A. Moshrefzadeh, A. Fasana, The Autogram: An effective approach for selecting the optimal demodulation band in rolling element bearings diagnosis, Mechanical Systems and Signal Processing 105 (2018) 294–318.

[37] P. Borghesani, P. Pennacchi, S. Chatterton, The relationship between kurtosis-and envelope-based indexes for the diagnostic of rolling element bearings, Mechanical Systems and Signal Processing 43 (1-2) (2014) 25–43.

[38] W. A. Smith, R. B. Randall, X. d. C. du Mée, P. Peng, Use of cyclostationary properties to diagnose planet bearing faults in variable speed conditions, in: 10th DST group international conference on health and usage monitoring systems, 17th Australian aerospace congress, 2017, pp. 26–28.

[39] A. Mauricio, W. Smith, R. Randall, J. Antoni, K. Gryllias, Cyclostationary-based tools for bearing diagnostics, Online Proceedings of ISMA2018 including USD2018 (2018) 905–918.

[40] A. Mauricio, W. Smith, J. Qi, R. Randall, K. Gryllias, Cyclo-non-stationary based bearing diagnostics of planetary gearboxes, in: International Conference on Condition Monitoring of Machinery in Non-Stationary Operation, Springer, 2018, pp. 343–352.

[41] S. Schmidt, P. S. Heyns, K. C. Gryllias, A pre-processing methodology to enhance novel information for rotating machine diagnostics, Mechanical Systems and Signal Processing 124 (2019) 541–561.

[42] W. A. Smith, P. Borghesani, Q. Ni, K. Wang, Z. Peng, Optimal demodulation-band selection for envelope-based diagnostics: A comparative study of traditional and novel tools, Mechanical Systems and Signal Processing 134 (2019) 106303.

[43] S. Schmidt, P. S. Heyns, K. C. Gryllias, A methodology using the spectral coherence and healthy historical data to perform gearbox fault diagnosis under varying operating conditions, Applied Acoustics 158 (2020) 107038.

[44] J. Antoni, Cyclic spectral analysis in practice, Mechanical Systems and Signal Processing 21 (2007) 597–630.

[45] J. Antoni, G. Xin, N. Hamzaoui, Fast computation of the spectral correlation, Mechanical Systems and Signal Processing 92 (2017) 248–277.

[46] P. Borghesani, J. Antoni, A faster algorithm for the calculation of the fast spectral correlation, Mechanical Systems and Signal Processing 111 (2018) 113–118.

[47] S. Kass, A. Raad, J. Antoni, Self-running bearing diagnosis based on scalar indicator using fast order frequency spectral coherence, Measurement 138 (2019) 467–484.

[48] J. Antoni, Cyclostationarity by examples, Mechanical Systems and Signal Processing 23 (4) (2009) 987–1036.

[49] J. Antoni, P. Borghesani, A statistical methodology for the design of condition indicators, Mechanical Systems and Signal Processing 114 (2019) 290–327.

[50] D. H. Diamond, P. S. Heyns, A. J. Oberholster, Online shaft encoder geometry compensation for arbitrary shaft speed profiles using Bayesian regression, Mechanical Systems and Signal Processing 81 (2016) 402–418.